The capacity of the human iliotibial band to store elastic energy during running

The capacity of the human iliotibial band to store elastic energy during running

Carolyn M. Eng[1,2], Allison S. Arnold[1], Daniel E. Lieberman[2], Andrew A. Biewener[1]

[1]*Department of Organismic and Evolutionary Biology, Harvard University, Cambridge, MA*

[2]*Department of Human Evolutionary Biology, Harvard University, Cambridge, MA*

Journal of Biomechanics

Original Article

Word Count: 4008 words

Keywords: Elastic energy storage, iliotibial band, fascia, musculoskeletal modeling

Correspondence to: Carolyn M. Eng, Department of Ecology and Evolutionary Biology, Brown University, PO Box G-B204, Providence, RI 02912. E-mail: carolyn_eng@brown.edu.

Abstract

The human iliotibial band (ITB) is a poorly understood fascial structure that may contribute to energy savings during locomotion. This study evaluated the capacity of the ITB to store and release elastic energy during running, at speeds ranging from 2-5 m/s, using a model that characterizes the three-dimensional musculoskeletal geometry of the human lower limb and the force-length properties of the ITB, tensor fascia lata (TFL), and gluteus maximus (GMax). The model was based on detailed analyses of muscle architecture, dissections of 3-D anatomy, and measurements of the muscles' moment arms about the hip and knee in five cadaveric specimens. The model was used, in combination with measured joint kinematics and published EMG recordings, to estimate the forces and corresponding strains in the ITB during running. We found that forces generated by TFL and GMax during running stretch the ITB substantially, resulting in energy storage. Anterior and posterior regions of the ITB muscle-tendon units (MTUs) show distinct length change patterns, in part due to different moment arms at the hip and knee. The posterior ITB MTU likely stores more energy than the anterior ITB MTU because it transmits larger muscle forces. We estimate that the ITB stores about 1 J of energy per stride during slow running and 7 J during fast running, which represents approximately 14% of the energy stored in the Achilles tendon at a comparable speed. This previously unrecognized mechanism for storing elastic energy may be an adaptation to increase human locomotor economy.

Introduction

Because bipedalism is a fundamental derived feature of hominins (species more closely related to humans than chimpanzees), many distinctive features of the human spine and lower extremity are adaptations to improve bipedal locomotor performance. Many adaptations for standing and walking, for example, appear early in hominin evolution including a inferiorly-oriented foramen magnum, a lordotic lumbar spine, and a sagittally-oriented ilium (see Aiello and Dean, 1990; Zollikofer et al., 2005). Additional features that first appear later in the genus *Homo* may reflect selection for endurance running, including a stabilized sacroiliac joint, an expanded attachment of gluteus maximus, and shorter toes (Bramble and Lieberman, 2004; Lieberman et al., 2006; Rolian et al., 2009). Although the selective factors underlying the evolution of both walking and running are debated, it is likely that locomotor economy played a key role. Hypothesized energy-saving features for walking include long legs and dorsally oriented ischia (Crompton et al., 1998; Pontzer et al., 2009; Robinson, 1972; Sockol et al., 2007). Energy saving features for running in the genus *Homo* include a long, compliant Achilles tendon and a spring-like median longitudinal arch, which are known to store and recover elastic energy during running in other vertebrates (Biewener, 2003; Ker et al., 1987; Roberts, 2002). In addition, the human lower extremity has a number of fascial structures with elastic properties that are not present in apes, but whether these structures store energy or serve another function remains poorly understood.

One of the most interesting of these structures is the iliotibial band (ITB). The ITB is a thickening of the lateral fascia of the thigh that originates on the pelvis and inserts on the tibia; it receives muscle fibers from the tensor fascia lata (TFL) anteriorly and

from the gluteus maximus (GMax) posteriorly (Gottschalk et al., 1989; Gray et al., 1995; Kaplan, 1958; Ober, 1936; Stern, 1972). The ITB is traditionally considered to function as a “strut” during walking, stabilizing the hip in the frontal plane (Gottschalk et al., 1989; Inman, 1947; Kaplan, 1958). However, the high compliance of the ITB (Butler et al., 1984; Derwin et al., 2008; Gratz, 1931), the fact that it crosses both the hip and knee, and the presence of in-series muscles suggest that the ITB may play other roles. If the ITB stretches substantially while transmitting muscle forces, storing elastic energy, then it may decrease the metabolic cost of locomotion. Prior studies have estimated that energy recovered from the Achilles tendon during running reduces muscle work by as much as 35% (Alexander and Bennet-Clark, 1977; Ker et al., 1987). Whether the ITB also stores and recovers elastic energy, and how this compares to Achilles tendon energy recovery, is unknown.

As a first step toward evaluating the ITB’s role in locomotor economy, this study examined the capacity of the ITB to store elastic energy at running speeds ranging from 2 to 5 m/s. We hypothesized that forces generated by TFL and GMax stretch the ITB during running, storing elastic energy that may be recovered later in the stride. We tested this hypothesis by developing a musculoskeletal model of the ITB and inserting muscles. Our model characterizes the 3-D skeletal geometry, the hip and knee kinematics, and the attachments and force-length (F-L) properties of the ITB, TFL and GMax for an average-sized adult male (femur length: 39.8 cm; tibia length: 36.2 cm). Because existing representations of TFL and GMax were not sufficiently accurate for this study, we performed detailed analyses of these muscles’ architecture and measured their moment arms (MAs) about the hip and knee in cadaveric specimens.

89 The TFL has largely been neglected in previous studies of muscle architecture (e.g.,
90 Ward et al., 2009; Wickiewicz et al., 1983) and locomotor function (e.g., Dorn et al.,
91 2012; Sasaki and Neptune, 2006), despite being active during running (Andersson et
92 al., 1997; Mann et al., 1986; Montgomery et al., 1994; Paré et al., 1981). GMax is
93 routinely modeled as a uniarticular hip extensor that inserts on the femur (e.g., Arnold et
94 al., 2010; Delp et al., 1990), despite evidence that a substantial portion of GMax inserts
95 on the ITB (Gray et al., 1995; Stern, 1972). Our refined musculoskeletal model, which
96 addresses these limitations, is available on SimTK (simtk.org). Using this model, we
97 estimated the forces transmitted to anterior and posterior regions of the ITB at body
98 positions corresponding to running, predicted the length changes of each region, and
99 calculated the corresponding ITB strain energies over the course of a stride based on
100 published measurements of the tissue's elastic modulus (Butler et al., 1984; Derwin et
101 al., 2008).
102
103 **Materials and methods**
104 *Muscle architecture measurements*
105 We characterized the isometric force-generating capacity of TFL and GMax
106 based on measurements of muscle architecture in three formalin-fixed human cadavers
107 (Table 1). Specimens were dissected and the muscles isolated and removed. Total
108 mass (*M*) of each muscle was measured; in addition, the masses of four regions of the
109 GMax were measured separately. A muscle fascicle was carefully dissected from each
110 region of GMax and from two regions of TFL and the fascicle lengths (L_f) measured.
111 Surface pennation angles between the fascicles and ITB were also measured. Under

112 magnification, muscle fiber bundles were isolated from each fascicle and mounted on
113 slides. Following Lieber et al. (1990), bundle sarcomere length (L_s') was determined by
114 laser diffraction and used to calculate optimal fascicle length (L_f):

115 $$L_f = L_f' \left(\frac{2.7 \mu m}{L_s'} \right) \quad (1)$$

116 where 2.7 μm is the optimal sarcomere length for human muscle (Lieber et al., 1994).
117 Physiological cross-sectional area (*PCSA*) was calculated from muscle mass and
118 optimal fascicle length (Powell et al., 1984):

119 $$PCSA = \frac{M}{\rho \cdot L_f} \quad (2)$$

120 where ρ is muscle density (1.056 g/cm^3; Mendez and Keyes, 1960). Our architecture
121 data for GMax are consistent with data reported by Ward et al. (2009).

122 *Muscle moment arm measurements*

123 We measured MAs of the muscle-ITB paths in five fresh frozen cadaveric hemi-
124 pelvises obtained from MedCure (Portland, OR). MAs were determined for hip
125 flex/extension, rotation, ab/adduction, and knee flex/extension using the tendon
126 excursion method (An et al., 1984; Brand et al., 1975). We approximated TFL with two
127 Kevlar thread paths (Figure 1A&B) and GMax with four paths (Figure 1A&C). The ITB
128 was left intact during these measurements. Each thread was anchored to a screw eye
129 at the path's insertion, routed over the ITB through plastic tubing to a screw eye at the
130 path's origin, and attached to one of two cable-extension position transducers (PTX101,
131 Celesco, Canoga Park, CA) that measured length changes with an accuracy of ±0.32
132 mm while applying a tension of 1.4 or 2.8 N. The tubing ensured a repeatable path

along the surface of the ITB and decreased friction. Detailed procedures for defining each path are described in supplementary materials.

Hip and knee angles were measured simultaneously with muscle-ITB length changes using a motion tracking system (Polhemus Fastrak, Colchester, VT) and custom software (LabView, National Instruments Corporation, Austin, TX). Receivers were rigidly attached to the pelvis, femur, and tibia to track the segments' positions and orientations. Segment coordinate systems were defined along anatomical axes by digitizing bony landmarks and determining the hip center (Figure S1), as described in the supplementary materials. For each muscle-ITB path, we digitized the origin, insertion and key "via" points that constrained the path with hip or knee motion. We also tracked the relative motions of nine marker pairs sutured along the ITB using high-speed video. These data guided development of the model and were analyzed to determine the hip and knee angles at which the anterior and posterior ITB began to stretch.

Each specimen was mounted in a custom frame (Figure 2) that allowed independent control of hip flex/extension, rotation, ab/adduction, and knee flexion following Arnold et al. (2000). Alignment and mounting of the specimen comprised four main steps, each performed with real-time feedback to ensure that the pelvis, femur, and tibia were secured to within 5 mm and 2° of the desired alignment. First, the pelvis was secured to a table and aligned with either its medial-lateral axis (for flex/extension MAs) or anterior-posterior axis (for ab/adduction MAs) perpendicular to the table. Second, the femur was mounted on a cart equipped with two concentric rings. The femur was secured to the inner ring so that the femur's long axis (from hip center to the

midpoint between femoral epicondyles) was centered perpendicular to the plane of the rings. Third, the base of the cart was adjusted so that its wheels rolled in an arc about the specimen's hip center. Fourth, the tibia was secured to a locking hinge attached to the inner ring. When measuring knee MAs, the hinge was removed and the tibia was flexed and extended. When measuring hip rotation MAs, the inner ring was rotated relative to the outer ring, which internally and externally rotated the hip. When measuring hip flex/extension or ab/adduction MAs, the cart was rotated about the specimen's hip center, thereby flex/extending or ab/adducting the hip. When measuring MAs about one axis, the other axes were locked in a neutral position (hip flexion = 0°, hip rotation = 5°, hip adduction = 0°, knee flexion = 0°). To verify alignment, we monitored coupling of hip angles and ensured that hip adduction varied < 2° and hip rotation < 4° over a 75° range of flexion. When the specimen was aligned for hip ab/adduction, we ensured that hip flexion varied < 2° and hip rotation < 4° over a 50° range of ab/adduction.

To measure muscle-ITB MAs, the excursion of each thread path was recorded while slowly moving the specimen through its ranges of hip and knee motion. Excursion and joint angle data were sampled at 10 Hz (National Instruments BNC-2090 A/D converter). The lengthening excursion versus joint angle data were fit with a fourth order polynomial, and the derivative of the polynomial was averaged across trials to estimate the MA. A minimum of five trials was collected for each condition.

Following MA measurements, muscles were freed, cleaned of fat and connective tissue, and weighed (Table 2). In two specimens, the regions of GMax were carefully

dissected to determine the relative masses of the portions that insert on the ITB versus the femur.

Model of TFL, Gmax, and ITB F-L properties

We modified the paths of TFL and GMax muscle-tendon units (MTUs) in the model reported by Arnold et al. (2010) to match our digitized attachments and MA data (Figure 3). Using SIMM (*Software for Interactive Musculoskeletal Modeling*, v7.0, MusculoGraphics, Santa Rosa, CA), we initially created two paths for TFL and eight for GMax (four to the ITB and four to the femur). Via points and wrapping surfaces were iteratively adjusted so that the model's paths reproduced the three-dimensional paths digitized during the experiments and the model's MAs matched the experimentally determined MAs. Because the model's MAs are extremely consistent with our experimental data (Figures 4 & S2), we are confident that the model accurately predicts length changes of these MTUs.

To estimate strain in regions of the ITB during running, we created three additional MTUs, representative of the major paths of ITB force transmission determined from our experiments (Figure 3B,C). One path accounts for force transmitted by the anterior ITB when TFL is active (TFL-ITB_{ant}). The other paths account for the cumulative force transmitted by the posterior ITB when superior (GMax1,2-ITB_{post1}) or inferior (GMax3,4-ITB_{post2}) portions of GMax are active. Attachments and via points of each path were iteratively adjusted to yield average MAs of the combined MTUs (Figures 4). This model represents the muscles as independent, proximal-to-distal MTUs, even though the ITB is multi-layered and loaded from different directions, based on detailed dissections and on biaxial testing of goat fascia lata, which showed

that the fascia's material properties are not strongly influenced by its biaxial strain environment (Eng et al., 2014).

We used a Hill-type muscle model (Delp et al., 1990; Zajac, 1989) to estimate isometric forces generated by TFL-ITB$_{ant}$, GMax1,2-ITB$_{post1,}$ and GMax3,4-ITB$_{post2}$ at different activation levels. Two parameters, maximum isometric force (F_{max}) and optimal fiber length (L_{opt}), scaled normalized active and passive F-L curves to each muscle (Table S1). F_{max} and an additional parameter, tendon slack length (L_{TS}), scaled a normalized "tendon" F-L curve to each MTU. We specified parameters for each MTU based on our architecture measurements and data reported by Ward et al. (2009). We adjusted L_{TS} such that ITB$_{ant}$ and ITB$_{post}$ began to stretch passively at hip and knee angles consistent with our experimental data.

For each MTU, we created a normalized F-L curve for the ITB (Figure 5) based on published material properties of the human ITB (Butler et al., 1984; Derwin et al., 2008). We assumed a transition strain of 4% based on data from goat fascia lata (Eng et al., 2014). Above 4% strain, we assumed a linear relationship between force and strain with a normalized stiffness ($\tilde{k}$) determined using the ITB's elastic modulus (E), the muscle's F_{max}, and the ITB's effective cross-sectional area (a):

$$\tilde{k} = \frac{E \times a}{F_{\max}}$$

The effective cross-sectional area of the ITB was calculated from measurements of thickness and width in cadaveric specimens (see Table S2). The width of each ITB region was measured while placing tension on the inserting muscle and visually assessing ITB strain. We used an elastic modulus of 400 MPa, which is consistent with values reported in the literature (Butler et al., 1984; Derwin et al., 2008; Hammer et al.,

2012; Steinke et al., 2012). Below 4% strain, in the toe region, we decreased stiffness by a factor of 2/3. At $F_{max,}$ the ITB strains 5-11% in our model, which seems plausible given the range of yield strains reported in the literature (10-27%; (Butler et al., 1984; Hammer et al., 2012; Hinton et al., 1992). The regional variation in strain at F_{max} is consistent with our measurements of ITB thickness, which are relatively uniform in anterior and posterior regions despite the fact that the inserting muscles differ substantially in force-generating capacity.

Assessment of ITB energy storage

We used our model in combination with published joint kinematics and EMG recordings to examine the capacity of the ITB to store elastic energy during running. First, we calculated the lengths of the MTUs at hip and knee angles corresponding to running using data from 10 experienced runners, at speeds of 2, 3, 4, and 5 m/s (Hamner and Delp, 2013). Next, we divided MTU lengths into muscle fiber lengths and ITB lengths by independently activating each MTU in the model and solving for the lengths at which the muscle and ITB forces were equivalent, accounting for pennation angle. Maximum activation levels for running were assumed to range between 20% and 65% of the EMG activation measured during a maximum voluntary contraction (MVC). In particular, we set each muscle's maximum activation to 20%, 35%, 50%, or 65% to estimate ITB strains during running at 2, 3, 4, and 5 m/s, respectively. These values are based on reported maximum activations of 20% MVC in GMax and TFL during level walking (Perry, 1992), 40% MVC in GMax and TFL during level running at 4.0 m/s (Montgomery et al., 1994), and 65% MVC in GMax during level running at 4.5 m/s (Swanson and Caldwell, 2000). Time-varying patterns of activity were derived from

EMG recordings reported for GMax and TFL (Jönhagen et al., 1996; Montgomery et al., 1994; Paré et al., 1981; Swanson and Caldwell, 2000), which we scaled to the maximum activation at each speed (Figure 7). Lastly, we estimated energy storage capacity at each speed by integrating the ITB F-L curves from L_{TS} to peak ITB length during running. Length changes of the ITB were determined relative to slack length. Total elastic energy stored in the posterior ITB was calculated as the sum of the energies stored in GMax1,2-ITB$_{post1}$ and GMax3,4-ITB$_{post2}$. We assessed the sensitivity of our analysis to the F-L properties by varying normalized stiffness by ±20% and transition strain by ±2% (Figure 5) and re-calculating energy storage.

Results

The TFL and GMax MTUs in our model undergo substantial excursions during running (Figure 6). Because of its hip flexion and knee extension MAs, TFL-ITB$_{ant}$ is maximally stretched during early swing, when the hip is extended and the knee flexed (Figure 3C). EMG recordings show that TFL is highly activated during this time (Figures 6 & 7) (Montgomery et al., 1994; Paré et al., 1981). In contrast, because of their role in hip extension and knee flexion MAs, GMax-ITB$_{post1}$ and GMax-ITB$_{post2}$ are maximally stretched during late swing, when the hip flexes and the knee extends (Figure 3C). EMG recordings show that GMax is highly activated during this time (Figures 6 & 7) (Jönhagen et al., 1996; Swanson and Caldwell, 2000). Inferior portions of GMax lengthen about 7% more than proximal portions, due to larger hip extension MAs when the hip is flexed.

The largest strains in ITB_{ant} occur in early swing (Figure 7A), with ITB_{ant} stretching 0.9 to 1.7 cm beyond slack length in our model. TFL muscle fiber length is longer than optimal when it begins generating force in late stance, and near optimal when it is maximally activated in early swing. Peak strains in ITB_{post} occur in late swing (Figure 7B), with ITB_{post} stretching 1.4 to 3.0 cm beyond slack length in our model. GMax3,4 is shorter than optimal length when it begins generating force in mid swing; however, it is stretched beyond optimal length as the hip flexes in swing. In late swing, when GMax3,4 is maximally activated, it operates near optimal length and generates forces that stretch ITB_{post} in our model. A similar pattern occurs in GMax1,2-ITB_{post2}. Passive strains in the ITB, without muscle activation, are relatively small in our model. ITB_{ant} strains 1.7% and ITB_{post} strains 1.1% over the stride cycle when the muscles are not activated.

Because the TFL and GMax MTUs are stretched to relatively long lengths when the muscles are active during running, both anterior and posterior regions of the ITB in our model have the capacity to store elastic energy. We estimate that ITB_{ant} strains about 4% during running at 5 m/s, which means that the ITB_{ant} may store nearly 1 J of energy per stride during early swing (Figure 8A). ITB_{post1} and ITB_{post2} strain about 4% during slow running and 7% during faster running in late swing when GMax is maximally active in our model. These data suggest that the ITB_{post} may store as much as 6 J per stride during late swing (Figure 8B).

Discussion

This is the first study to quantitatively characterize the 3-D musculoskeletal geometry of the human ITB and its inserting muscles. Dissections confirmed that all

fibers of TFL insert into the anterior ITB and a large fraction of GMax (40-70% by mass) inserts into the posterior ITB. Thus, the ITB likely transmits substantial force. Additionally, our MA measurements confirmed that the inserting muscles have relatively large MAs about the hip, and thus undergo large MTU excursions, with hip flexion and extension. In combination, the ITB's high compliance and its potential to transmit force while changing length, suggest a plausible, previously unrecognized mechanism for storing elastic energy during running.

We created a model that characterizes the geometry and F-L properties of the ITB, TFL, and GMax to test the hypothesis that forces generated by TFL and GMax stretch the ITB during running, storing elastic energy. Analysis of the model revealed that the ITB has the capacity to store 7 J per stride during running at 5 m/s. The posterior ITB stores substantially more energy than the anterior ITB because it transmits larger muscle forces.

How does the amount of energy stored in the ITB during running compare to energy stored in the Achilles tendon? Using a 3-D model and static optimization, Lai et al. (2014) estimated that the soleus and gastrocnemius store 40-50 J per stride in the Achilles tendon at slow to fast running speeds (3.5 – 5 m/s), an estimate consistent with previous experimental studies (Alexander and Bennet-Clark, 1977; Hof et al., 2002; Ker et al., 1987). We therefore calculate that the combined anterior and posterior ITB stores 14% as much energy as the Achilles tendon at a 5 m/s pace.

To provide additional context, we compared energy stored in the ITB to hip muscle work during running. Sasaki and Neptune (2006) used a muscle-driven dynamic simulation to estimate the mechanical work performed by hip muscles and series elastic

315 elements during running at 2.4 m/s. They reported that the hip extensors do 40 J of
316 work per stride during stance, while the hip flexors do 6 J of work during swing.
317 Recovery of 2 J from ITB_{post} during slow running could account for 5% of the work done
318 by hip extensors in stance, while recovery of 0.3 J from ITB_{ant} could contribute 5% of the
319 work done by hip flexors in swing. Although the extent to which energy recovery would
320 drive selection for endurance running is unknown, these comparisons suggest that
321 energy storage in the ITB is not negligible.

322 This analysis has several limitations. First, although our data confirm that forces
323 generated by TFL and GMax stretch the ITB during running, storing useful energy, our
324 study did not test whether the human ITB reduces muscle work or enhances locomotor
325 economy. Second, uncertainty exists in the parameters used to derive the F-L curves.
326 For example, our measures of ITB width and thickness in cadaveric specimens may not
327 be representative of healthy young subjects, thus potentially underestimating ITB
328 stiffness. However, varying normalized stiffness by ±20% and transition strain by ±2%
329 altered our estimates of energy storage by only 0.1 J in the anterior ITB and by 1.2 J in
330 the posterior ITB at the fastest running speed. At the slowest running speed, varying
331 stiffness and transition strain altered our estimates of energy storage by about 0.05 J.
332 Thus, we are reasonably confident in our model of the ITB's force-strain behavior and
333 that the ITB contributes to energy storage at all running speeds. Third, we estimated the
334 peak forces generated by TFL and GMax ignoring the muscles' force-velocity (F-V)
335 properties and assuming the muscles' activation patterns during running. If the muscles
336 shorten substantially during running, or if we overestimated activation, then we likely
337 overestimated ITB energy storage. It is plausible, however, that the ITB's length and

compliance allow GMax to operate nearly isometrically when generating maximum force in late stance, mitigating the effects of F-V properties on muscle-ITB mechanics. In the running simulations described by Lai et al. (2014), muscles inserting on the Achilles tendon contracted nearly isometrically across a range of running speeds. Lastly, we estimated the capacity of the ITB to store elastic energy during running but not walking. It is likely that the ITB transmits smaller forces, and thus stores less energy, during walking than reported here.

Our study has implications for understanding the evolution of human bipedalism. While these data do not exclude the possibility that the ITB stores substantial energy during walking, selection for the capacity to run long distances would have presented unique demands on the anatomy and physiology of *Homo* (see Bramble and Lieberman (2004) for review). Among these demands is the need to efficiently accelerate the swing limb, which is long and massive in humans (14% body mass) compared to chimpanzees (9% body mass; Zihlman and Brunker, 1979). The human ITB is stretched substantially just before swing, when the TFL is active and the hip is extending (Figures 6 & 7). Subsequent recoil of the ITB may help accelerate the swing limb. Although the energetic cost of running is primarily determined by muscle forces that support the body during stance (Kram and Taylor, 1990), the cost of accelerating the swing limb may be as much as 27% of total metabolic cost (Marsh et al., 2004; Modica and Kram, 2005; Myers and Steudel, 1985). Thus, selection for increased running economy may have favored traits that increase swing phase energy recovery in *Homo*. The need to decrease locomotor costs may also help explain the expansion of GMax evident in *Homo*. This adaptation is thought to play a role in trunk stabilization during endurance

running (Lieberman et al., 2006), but it may also facilitate elastic energy storage by increasing the forces transmitted to the ITB as it is stretched in late swing.

Acknowledgements

The authors fondly remember Farish A. Jenkins Jr. (1940-2012) for many stimulating and insightful discussions. Professor Jenkins helped guide C.M.E.'s dissertation research, which provided the basis for this study, and he deserves much credit. The authors thank two anonymous reviewers for constructive comments that significantly improved this manuscript. We gratefully acknowledge Delande Justinvil and Zachary Lewis for technical assistance during the moment arm experiments. We thank Casey Boyle and Yasmin Rawlins for assistance during pilot studies, and we thank Andrew Mountcastle and Glenna Clifton for help with videography. We are grateful to Tom Roberts for helpful comments on a preliminary version of the manuscript. This research was funded by a Wenner-Gren Dissertation Fieldwork Grant to C.M.E. under award no. 8588.

Figure legends

Figure 1. A: Lateral view of the human ITB showing paths of the inserting muscles, TFL and GMax, as characterized during the moment arm measurements. B: Lateral diagram showing the anterior and posterior paths of TFL. C: Posterior diagram showing the superior (Gmax1,2) and inferior (GMax3,4) regions of GMax. Muscle-ITB paths are described in the supplementary materials.

Figure 2. Hardware and procedure for measuring hip ab/adduction and rotation moment arms. The hardware consisted of a fixed table for aligning and securing the pelvis, an adjustable cart for moving the femur through a range of hip ab/adduction angles, and a set of concentric rings for rotating the femur about its mechanical axis, following Arnold et al. (2000). Receivers (shown in gray) were rigidly attached to the pelvis, femur, and tibia to track their motions in real time. 1: The pelvis was secured to a fixed table with its anterior-posterior axis perpendicular to the table. 2: The femur was secured to the inner of the two rings so that the femur's long axis was centered perpendicular to the plane of the rings. 3: The bases of the cart were adjusted so that the cart's wheels rolled in an arc about the specimen's hip joint center. 4: The tibia was secured to a locking hinge. Hip flex/extension moment arms were measured by re-orienting the pelvis on the table so that its medial-lateral axis was perpendicular to the table. More details are provided in the supplementary materials.

Figure 3. Lower extremity model modified from Arnold et al. (2010). A: Lateral view showing the two TFL-ITB paths that reproduce our experimental data. B: Posterior view showing the four GMax-ITB paths originating on the ilium, sacrum, and coccyx and inserting on the ITB. C: Lateral view of the combined MTU paths used to estimate energy storage. TFL-ITB_{ant}, GMax1,2-ITB_{post1}, and GMax3,4-ITB_{post2} paths are shown at touchdown, midstance, toeoff, and midswing during running at 5 m/s. The TFL-ITB_{ant} MTU is maximally stretched in early swing, while the GMax-ITB_{post} MTUs are most stretched during late swing.

Figure 4. Hip and knee moment arms of TFL-ITB_{ant} and GMax-ITB_{post} compared with experimental data. A: TFL has a large hip flexion MA that increases as the hip flexes. B: TFL has a large hip abduction MA that increases with hip abduction. C: The most posterior part of TFL has a small knee extension MA that decreases with knee flexion. D,G: All portions of GMax that insert on the ITB have large hip extension MAs. E: The superior portions of GMax have hip abduction MAs. H: The inferior portions of GMax have hip adduction MAs. F,I: The portions of GMax that insert on the ITB have small knee flexion MAs. Solid lines and shaded regions indicate the means and standard deviations of experimentally determined MAs from five cadaveric limbs. A-C: Dashed lines show the MAs of TFL1-ITB (dark gray), TFL2-ITB (light gray), and the combined TFL1,2-ITB_{ant} (black) predicted by our model. D-I: Dashed lines show the MAs (from superior to inferior) of GMax1 (dark gray), GMax2 (light gray), GMax3 (dark gray), GMax4 (light gray), and the combined paths for GMax1,2-ITB_{post1} (black, D-F) and GMax3,4-ITB_{post2} (black, G-I) as predicted by our model. Note the y-axes have different scales.

Figure 5. Normalized force-length curves for anterior and posterior regions of the ITB derived from experimental data (Butler et al., 1984; Derwin et al., 2008; Eng et al., 2014). Curves are shown for TFL-ITB$_{ant}$ (short dash), GMax1,2-ITB$_{post1}$ (long dash), and GMax3,4-ITB$_{post2}$ (dot-dash) with shaded regions indicating ±20% stiffness used in the sensitivity analysis. The ITB is more compliant than tendon (solid line), as shown by the typical tendon force-length curve generated by Millard et al. (2013) and by ultrasound-based measures of tendon force-length properties reported by Magnusson et al. (2001; light gray). This figure is adapted from figure 3 in Millard et al. (2013).

Figure 6. Length changes of TFL-ITB and GMax-ITB MTUs during fast running (5 m/s). TFL-ITB$_{ant}$ (light gray) stretches during stance phase, while GMax1,2-ITB$_{post1}$ (dark gray) and GMax3,4-ITB$_{post2}$ (black) stretch during the swing phase. Regions of intermediate muscle activity (10-30% activation; intermediately thickened portion of each curve) and maximal muscle activity (31-65% activation; thickened portion of each curve) demonstrate that these muscles are maximally active when the MTU is near maximum length.

Figure 7. TFL-ITB$_{ant}$ and GMax3,4-ITB$_{post}$ activation patterns over the stride cycle. For each muscle, the time-varying pattern was scaled to an activation level of 20%, 35%, 50%, or 65% during running at 2, 3, 4, and 5 m/s, respectively (increasingly darker lines). Filled squares on each line indicate toe-off. Superimposed are plots of force versus normalized fiber length and force versus ITB strain at key points in the gait cycle during running at 5 m/s. Circles on the curves show where the muscle or ITB is acting at that point in the gait cycle. A: TFL is longer than optimal length (L_{opt}) prior to toe-off when the muscle begins to generate force. When TFL is maximally activated in early swing, it operates near optimal length and stretches ITB$_{ant}$ to its longest length in our model. B: GMax3,4 is shorter than optimal length when it begins generating force in mid swing and is stretched beyond optimal length in swing. When GMax3,4 is maximally activated in late swing, it operates near optimal length and stretches ITB$_{post}$ to its longest length in our model.

Figure 8. Elastic energy stored in the ITB during running at 2, 3, 4, and 5 m/s as predicted by the model. A: Peak energy stored in ITB$_{ant}$ when TFL is activated 20, 35, 50, or 65%. B: Peak energy stored in ITB$_{post}$ when GMax is activated 20, 35, 50, or 65%. The energy stored in GMax-ITB$_{post}$ is calculated as the sum of energies stored in GMax1,2-ITB$_{post1}$ (gray) and GMax3,4-ITB$_{post2}$ (white).

References

Aiello, L.C., Dean, C., 1990. An Introduction to Human Evolutionary Anatomy. Academic Press, Boston.

Alexander, R.M., Bennet-Clark, H.C., 1977. Storage of elastic strain energy in muscle and other tissues. Nature 265, 114-117.

An, K.N., Takahashi, K., Harrigan, T.P., Chao, E.Y., 1984. Determination of muscle orientations and moment arms. Journal of Biomechanical Engineering 106, 280-282.

Andersson, E.A., Nilsson, J., Thorstensson, A., 1997. Intramuscular EMG from the hip flexor muscles during human locomotion. Acta Physiologica Scandinavica 161, 361-370.

Arnold, A.S., Salinas, S., Asakawa, D.J., Delp, S.L., 2000. Accuracy of muscle moment arms estimated from MRI-based musculoskeletal models of the lower extremity. Computer Aided Surgery 5, 108-119.

Arnold, E.M., Hamner, S.R., Seth, A., Millard, M., Delp, S.L., 2013. How muscle fiber lengths and velocities affect muscle force generation as humans walk and run at different speeds. Journal of Experimental Biology 216, 2150-2160.

Arnold, E.M., Ward, S.R., Lieber, R.L., Delp, S.L., 2010. A model of the lower limb for analysis of human movement. Annals of Biomedical Engineering 38, 269-279.

Biewener, A.A., 2003. Animal Locomotion. Oxford University Press, Oxford.

Bramble, D., Lieberman, D., 2004. Endurance running and the evolution of *Homo*. Nature 432, 345-352.

Brand, P.W., Cranor, K.C., Ellis, J.C., 1975. Tendon and pulleys at the metacarpophalangeal joint of a finger. Journal of Bone and Joint Surgery 57, 779-784.

Butler, D.L., Grood, E.S., Noyes, F.R., Zernicke, R.F., Brackett, K., 1984. Effects of structure and strain measurement technique on the material properties of young human tendons and fascia. Journal of Biomechanics 17, 579-596.

Crompton, R.H., Li, Y., Wang, W., Günther, M.M., Savage, R., 1998. The mechanical effectiveness of erect and “bent-hip, bent-knee” bipedal walking in *Australopithecus afarensis*. Journal of Human Evolution 35, 55-74.

Delp, S.L., Loan, J.P., Hoy, M.G., Zajac, F.E., Topp, E.L., Rosen, J.M., 1990. An interactive graphics-based model of the lower extremity to study orthopaedic surgical procedures. IEEE Transactions on Biomedical Engineering 37, 757-767.

Derwin, K.A., Baker, A.R., Spragg, R.K., Leigh, D.R., Farhat, W., Iannotti, J.P., 2008. Regional variability, processing methods, and biophysical properties of human fascia lata extracellular matrix. Journal of Biomedical Materials Research Part A 84, 500-507.

Dorn, T.W., Schache, A.G., Pandy, M.G., 2012. Muscular strategy shift in human running: dependence of running speed on hip and ankle muscle performance. Journal of Experimental Biology 215, 1944-1956.

Eng, C.M., Pancheri, F.Q., Lieberman, D.E., Biewener, A.A., Dorfmann, L., 2014. Directional differences in the biaxial material properties of fascia lata and the implications for fascia function. Annals of Biomedical Engineering 42, 1224-1237.

Gottschalk, F., Kourosh, S., Leveau, B., 1989. The functional anatomy of tensor fasciae latae and gluteus medius and minimus. Journal of Anatomy 166, 179-189.

Gratz, C.M., 1931. Tensile strength and elasticity tests on human fascia lata. The Journal of Bone and Joint Surgery 13, 334-340.

Gray, H., Williams, P.L., Bannister, L.H., 1995. Gray's Anatomy: The Anatomical Basis of Medicine and Surgery. Churchill Livingstone, Edinburgh.

Hammer, N., Lingslebe, U., Aust, G., Milani, T.L., Hädrich, C., Steinke, H., 2012. Ultimate stress and age-dependent deformation characteristics of the iliotibial tract. Journal of the Mechanical Behavior of Biomedical Materials 16, 81-86.

Hamner, S.R., Delp, S.L., 2013. Muscle contributions to fore-aft and vertical body mass center accelerations over a range of running speeds. Journal of Biomechanics 46, 780-787.

Hinton, R., Jinnah, R.H., Johnson, C., Warden, K., Clarke, H.J., 1992. A biomechanical analysis of solvent-dehydrated and freeze-dried human fascia lata allografts: A preliminary report. American Journal of Sports Medicine 20, 607-612.

Hof, A., Van Zandwijk, J., Bobbert, M., 2002. Mechanics of human triceps surae muscle in walking, running and jumping. Acta Physiologica Scandinavica 174, 17-30.

Inman, V.T., 1947. Functional aspects of the abductor muscles of the hip. The Journal of Bone and Joint Surgery 29, 607-619.

Jönhagen, S., Ericson, M., Nemeth, G., Eriksson, E., 1996. Amplitude and timing of electromyographic activity during sprinting. Scandinavian Journal of Medicine and Science in Sports 6, 15-21.

Kaplan, E.B., 1958. The iliotibial tract: Clinical and morphological significance. The Journal of Bone and Joint Surgery 40, 817-832.

Ker, R.F., Bennett, M.B., Bibby, S.R., Kester, R.C., Alexander, R.M., 1987. The spring in the arch of the human foot. Nature 325, 147-149.

Kram, R., Taylor, C.R., 1990. Energetics of running: A new perspective. Nature 346, 265-267.

Lai, A., Schache, A.G., Lin, Y.-C., Pandy, M.G., 2014. Tendon elastic strain energy in the human ankle plantar-flexors and its role with increased running speed. Journal of Experimental Biology 217, 3159-3168.

Lieber, R.L., Fazeli, B.M., Botte, M.J., 1990. Architecture of selected wrist flexor and extensor muscles. Journal of Hand Surgery 15A, 244-250.

Lieber, R.L., Loren, G.J., Fridén, J., 1994. In vivo measurement of human wrist extensor muscle sarcomere length changes. Journal of Neurophysiology 71, 874-881.

Lieberman, D.E., Raichlen, D.A., Pontzer, H., Bramble, D.M., Cutright-Smith, E., 2006. The human gluteus maximus and its role in running. Journal of Experimental Biology 209, 2143-2155.

579 Magnusson, S.P., Aagaard, P., Rosager, S., Dyre-Poulsen, P., Kjaer, M., 2001.
580 Load-displacement properties of human triceps surae aponeurosis *in vivo*. Journal of
581 Physiology (London) 531, 277-288.

582
583 Mann, R., Moran, G., Dougherty, S., 1986. Comparative electromyography of the
584 lower extremity in jogging, running, and sprinting. American Journal of Sports Medicine
585 14, 501-510.

586
587 Marsh, R.L., Ellerby, D.J., Carr, J.A., Henry, H.T., Buchanan, C.I., 2004.
588 Partitioning the energetics of walking and running: Swinging the limbs is expensive.
589 Science 303, 80-83.

590
591 Mendez, J., Keys, A., 1960. Density and composition of mammalian muscle.
592 Metabolism: Clinical and Experimental 9, 184-188.

593
594 Millard, M., Uchida, T., Seth, A., Delp, S.L., 2013. Flexing computational muscle:
595 Modeling and simulation of musculotendon dynamics. Journal of Biomechanical
596 Engineering 135, 1-11.

597
598 Modica, J.R., Kram, R., 2005. Metabolic energy and muscular activity required
599 for leg swing in running. Journal of Applied Physiology 98, 2126-2131.

600
601 Montgomery, W.H., Pink, M., Perry, J., 1994. Electromyographic analysis of hip
602 and knee musculature during running. American Journal of Sports Medicine 22, 272-
603 278.

604
605 Myers, M., Steudel, K., 1985. Effect of limb mass and its distribution on the
606 energetic cost of running. Journal of Experimental Biology 116, 363-373.

607
608 Ober, F.R., 1936. The role of the iliotibial band and fascia lata as a factor in the
609 causation of low-back disabilities and sciatica. The Journal of Bone and Joint Surgery
610 18, 105-110.

611
612 Paré, E., Stern, J., Schwartz, J., 1981. Functional differentiation within the tensor
613 fasciae latae. The Journal of Bone and Joint Surgery 63, 1457-1471.

614
615 Perry, J., 1992. Gait Analysis: Normal and Pathological Function. Slack Inc.,
616 Thorofare, NJ.

Pontzer, H., Raichlen, D.A., Sockol, M.D., 2009. The metabolic cost of walking in humans, chimpanzees, and early hominins. Journal of Human Evolution 56, 43-54.

Powell, P.L., Roy, R.R., Kanim, P., Bello, M., Edgerton, V.R., 1984. Predictability of skeletal muscle tension from architectural determinations in guinea pig hindlimbs. Journal of Applied Physiology 57, 1715-1721.

Roberts, T., 2002. The integrated function of muscles and tendons during locomotion. Comparative Biochemistry and Physiology-Part A: Molecular & Integrative Physiology 133, 1087-1099.

Robinson, J.T., 1972. Early Hominid Posture and Locomotion. University of Chicago Press, Chicago.

Rolian, C., Lieberman, D.E., Hamill, J., Scott, J.W., Werbel, W., 2009. Walking, running and the evolution of short toes in humans. Journal of Experimental Biology 212, 713-721.

Sasaki, K., Neptune, R.R., 2006. Muscle mechanical work and elastic energy utilization during walking and running near the preferred gait transition speed. Gait and Posture 23, 383-390.

Sockol, M.D., Raichlen, D.A., Pontzer, H., 2007. Chimpanzee locomotion energetics and the origin of human bipedalism. Proceedings of the National Academy of Sciences 104, 12265-12269.

Steinke, H., Lingslebe, U., Böhme, J., Slowik, V., Shim, V., Hädrich, C., Hammer, N., 2012. Deformation behavior of the iliotibial tract under different states of fixation. Medical Engineering and Physics 34, 1221-1227.

Stern, J.T., Jr., 1972. Anatomical and functional specializations of the human gluteus maximus. American Journal of Physical Anthropology 36, 315-339.

Swanson, S.C., Caldwell, G.E., 2000. An integrated biomechanical analysis of high speed incline and level treadmill running. Medicine and Science in Sports and Exercise 32, 1146-1155.

Ward, S.R., Eng, C.M., Smallwood, L.H., Lieber, R.L., 2009. Are current measurements of lower extremity muscle architecture accurate? Clinical Orthopaedics and Related Research 467, 1074-1082.

Wickiewicz, T.L., Roy, R.R., Powell, P.L., Edgerton, V.R., 1983. Muscle architecture of the human lower limb. Clinical Orthopaedics and Related Research 179, 275-283.

Zajac, F.E., 1989. Muscle and tendon: Properties, models, scaling, and application to biomechanics and motor control. Critical Reviews in Biomedical Engineering 17, 359-411.

Zihlman, A.L., Brunker, L., 1979. Hominid bipedalism: Then and now. Yearbook of Physical Anthropology 22, 132-162.

Zollikofer, C., Ponce de Leon, M., Lieberman, D., Guy, F., Pilbeam, D., Likius, A., Mackaye, H., Vignaud, P., Brunet, M., 2005. Virtual reconstruction of *Sahelanthropus tchadensis*. Nature 434, 755-759.

Figure 1

Click here to download high resolution image

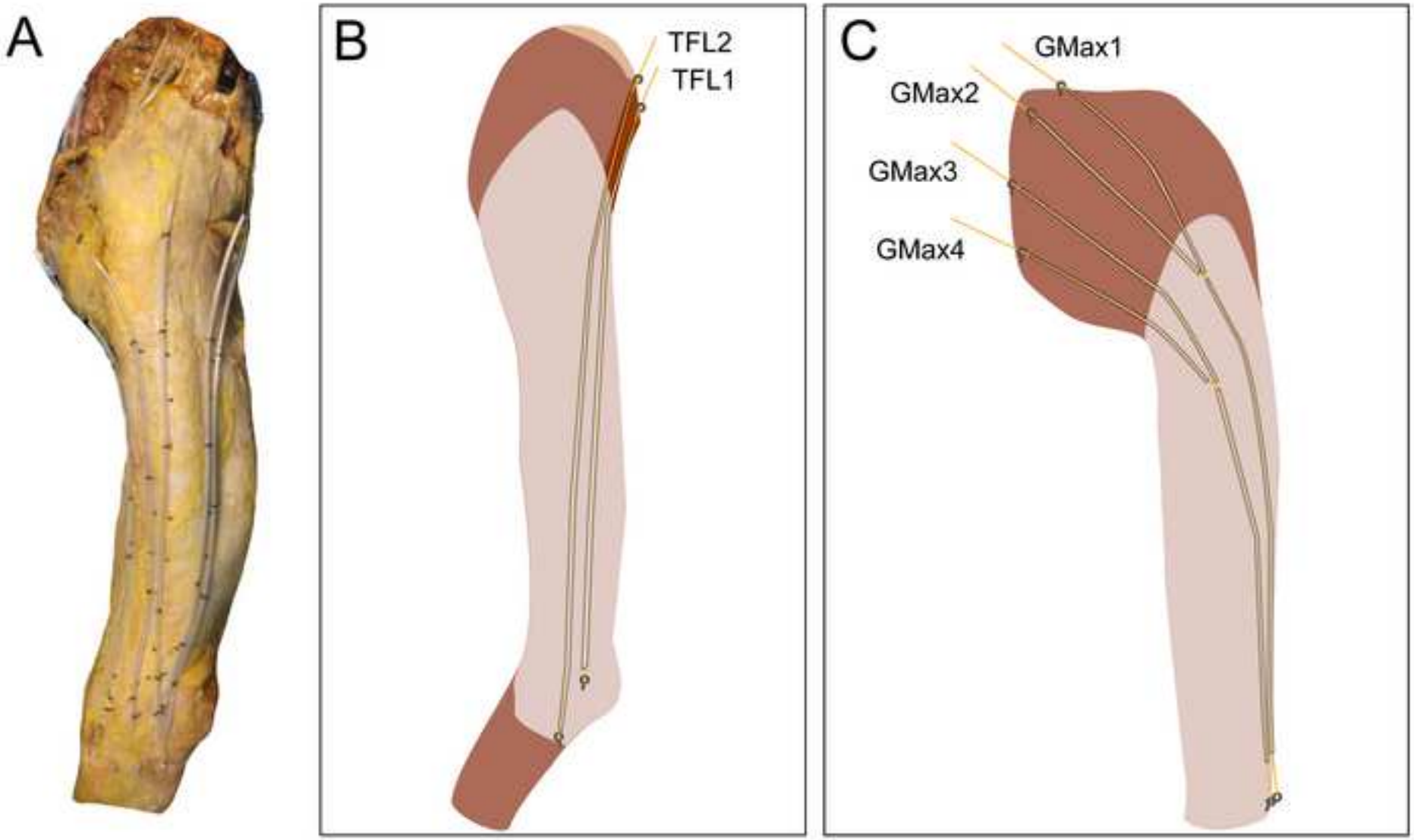

Figure 2

Click here to download high resolution image

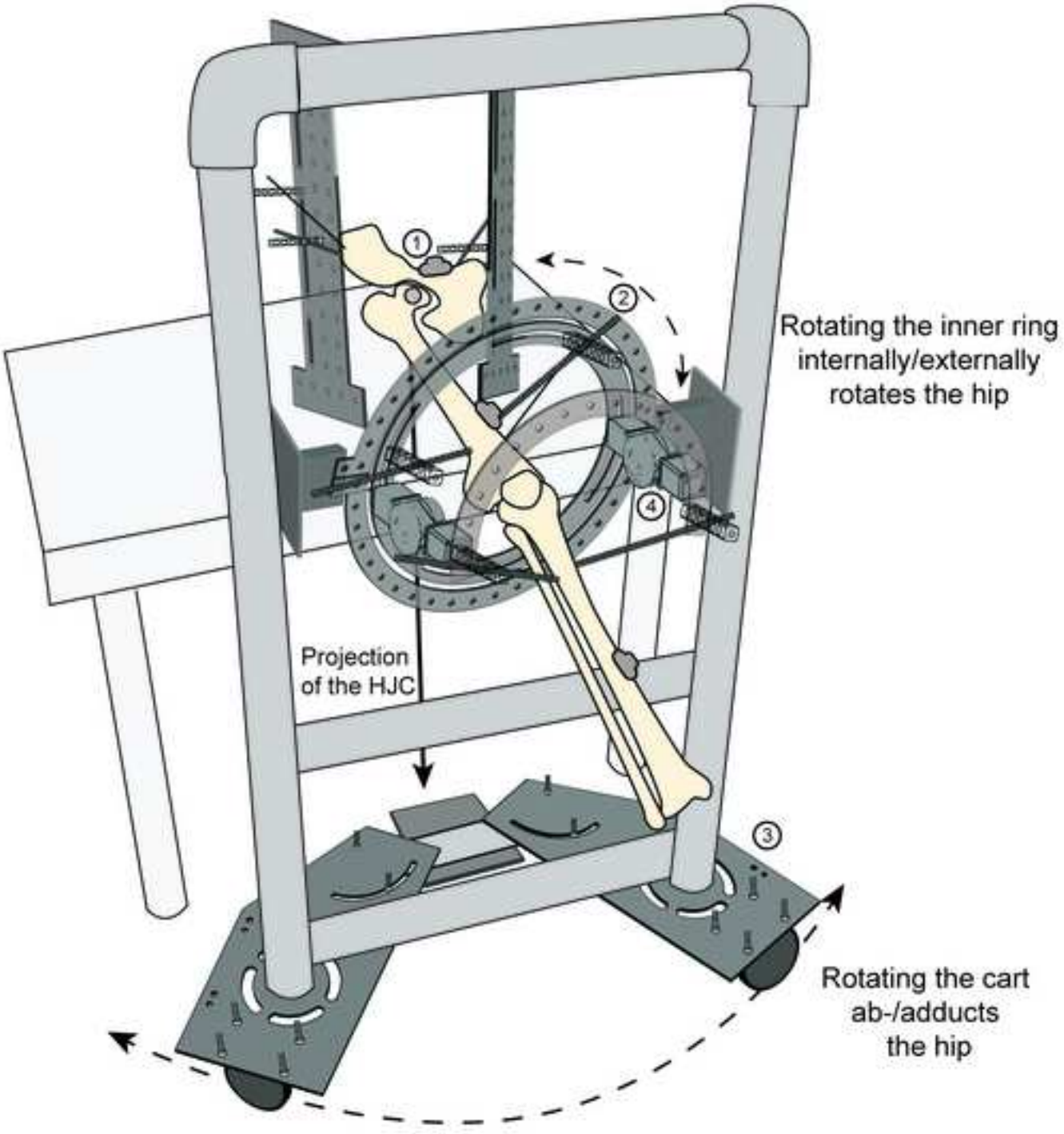

Figure 3

Click here to download high resolution image

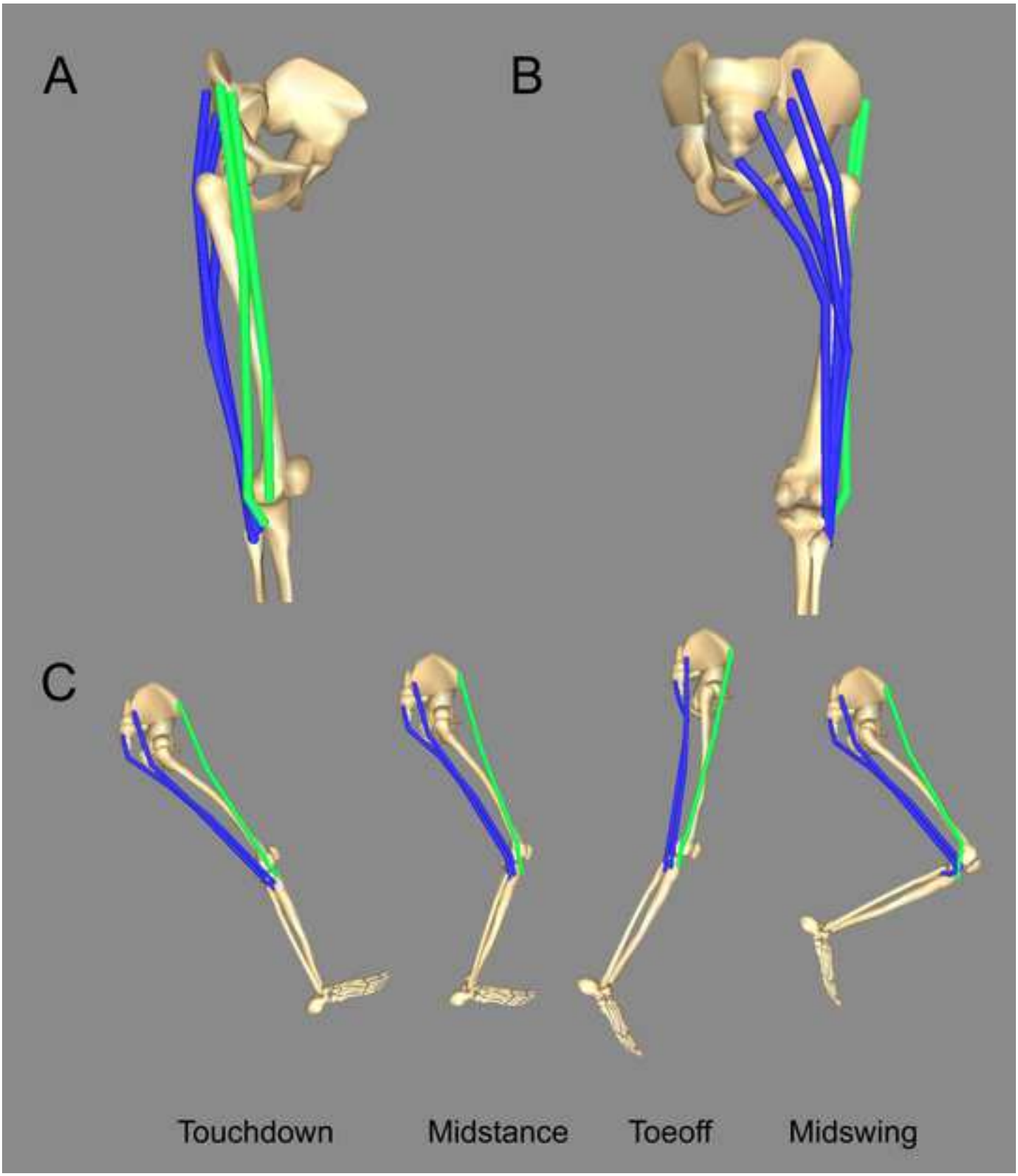

Figure 4

Click here to download high resolution image

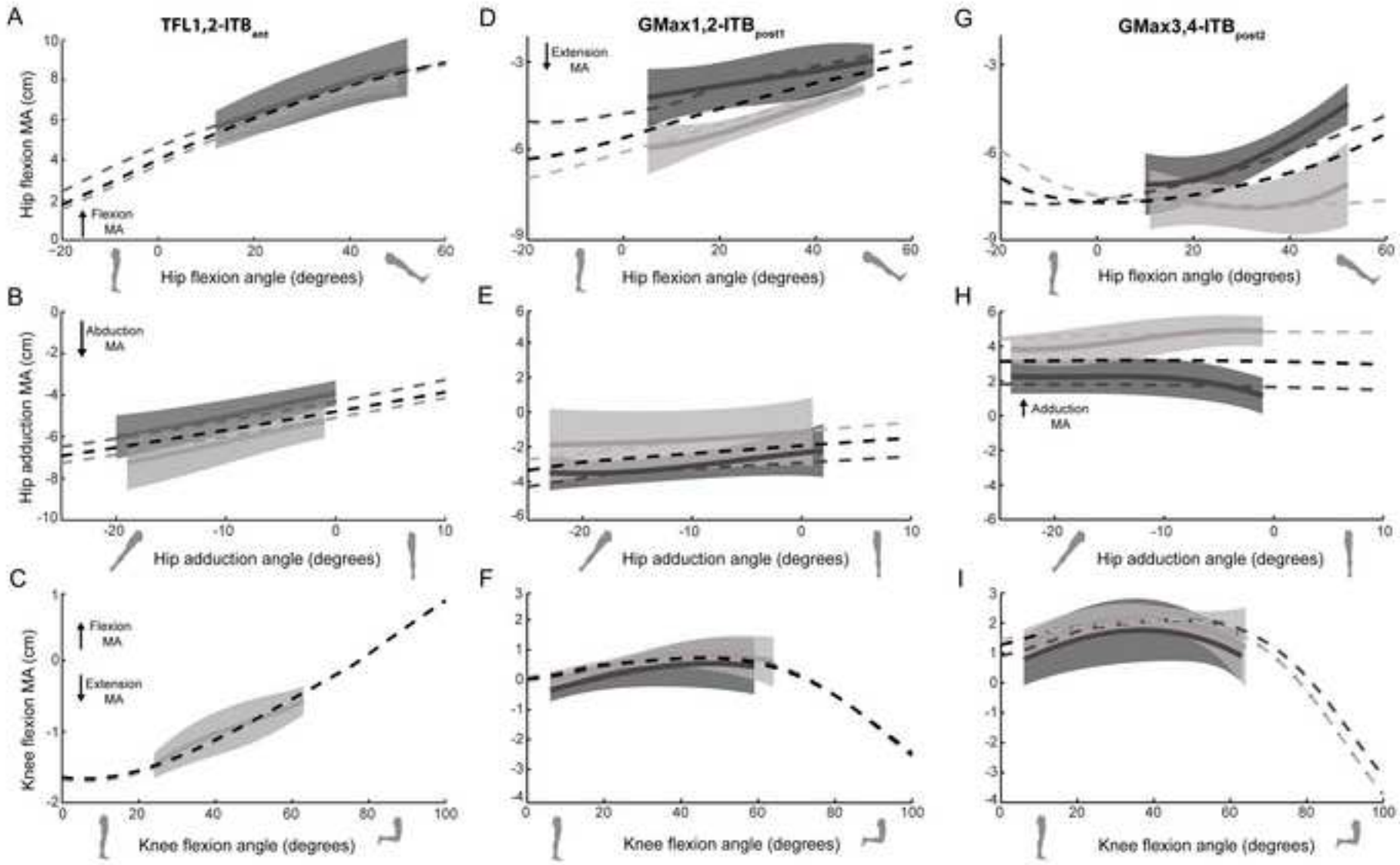

Figure 5

Click here to download high resolution image

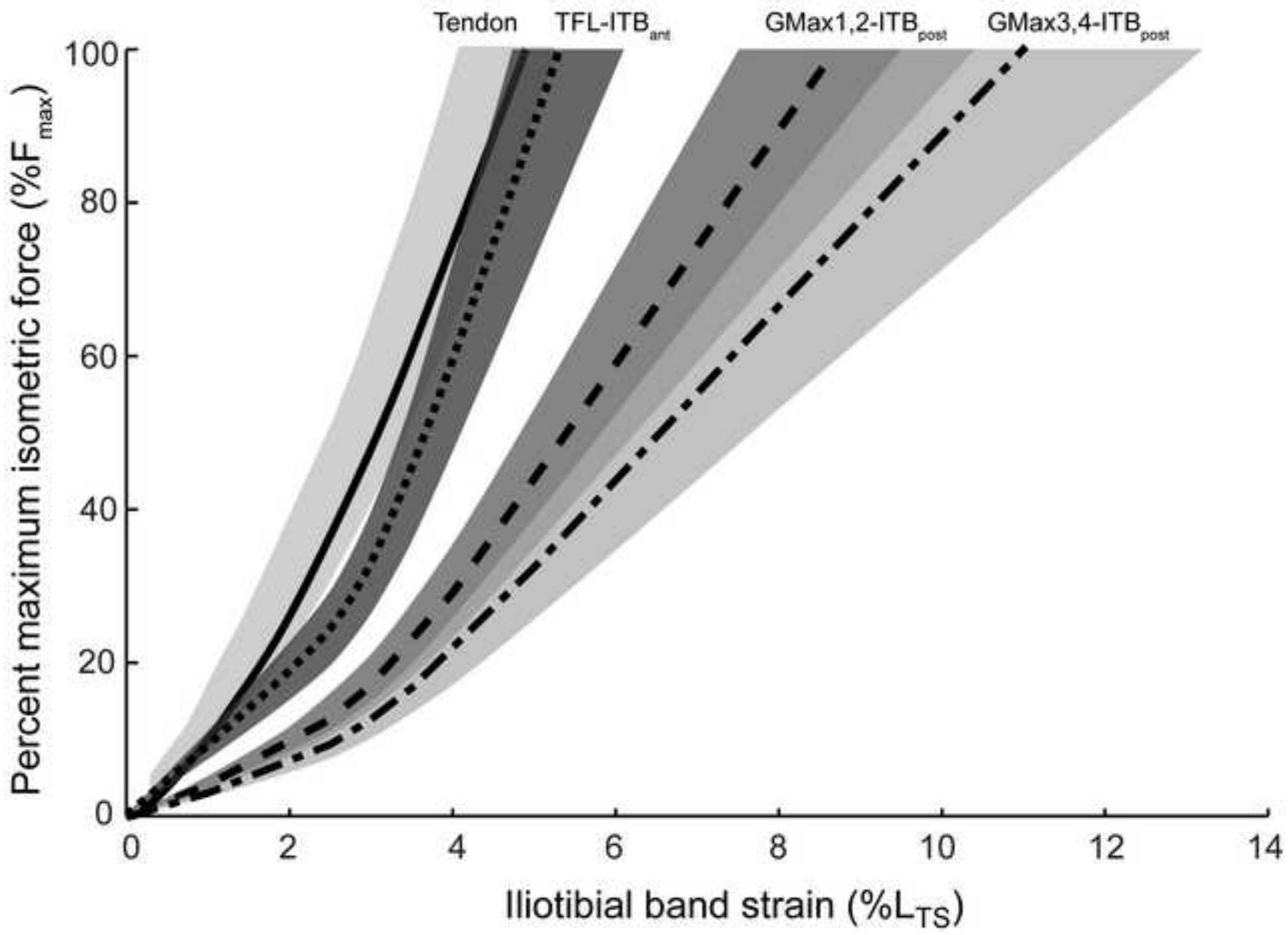

Figure 6

Click here to download high resolution image

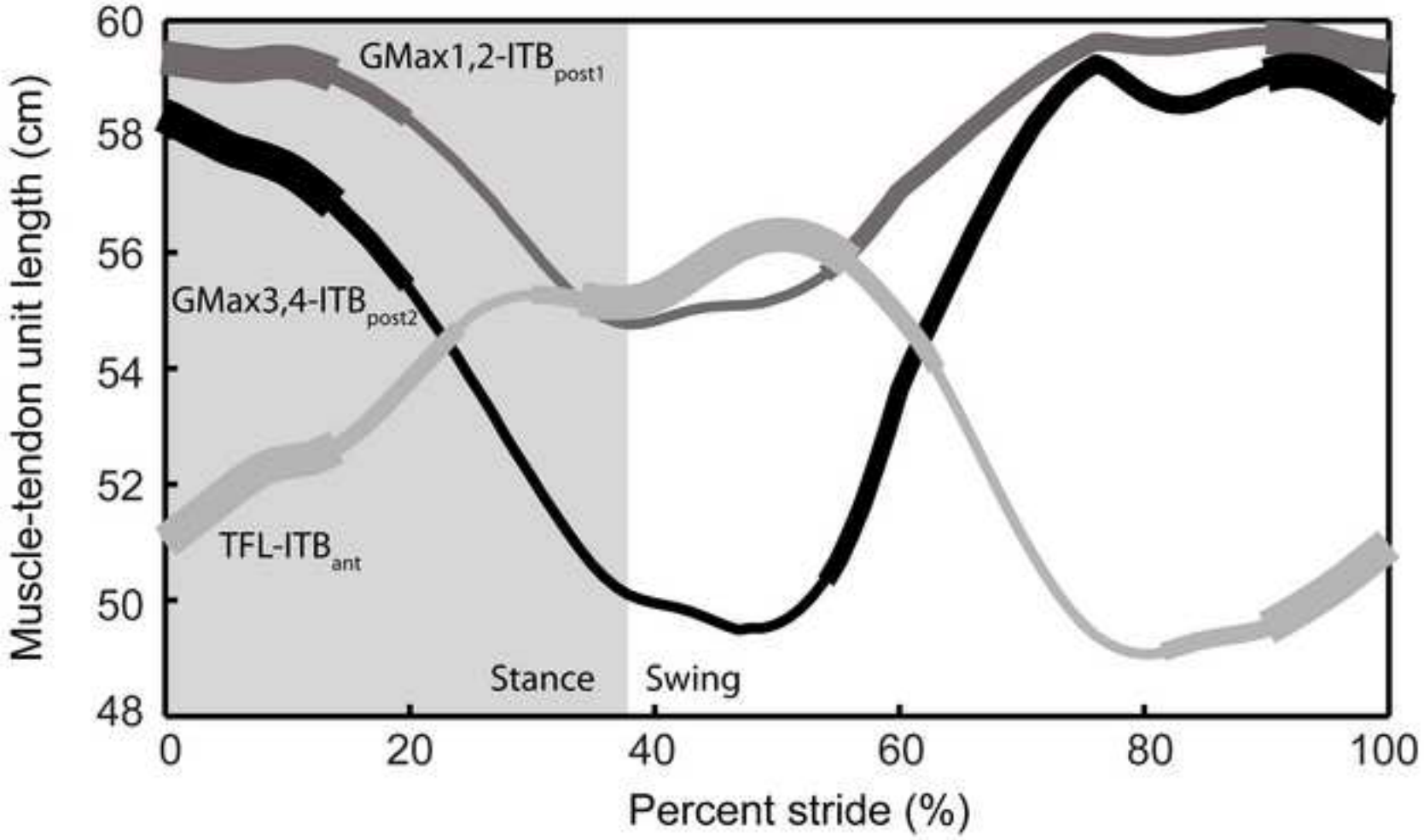

Figure 7

Click here to download high resolution image

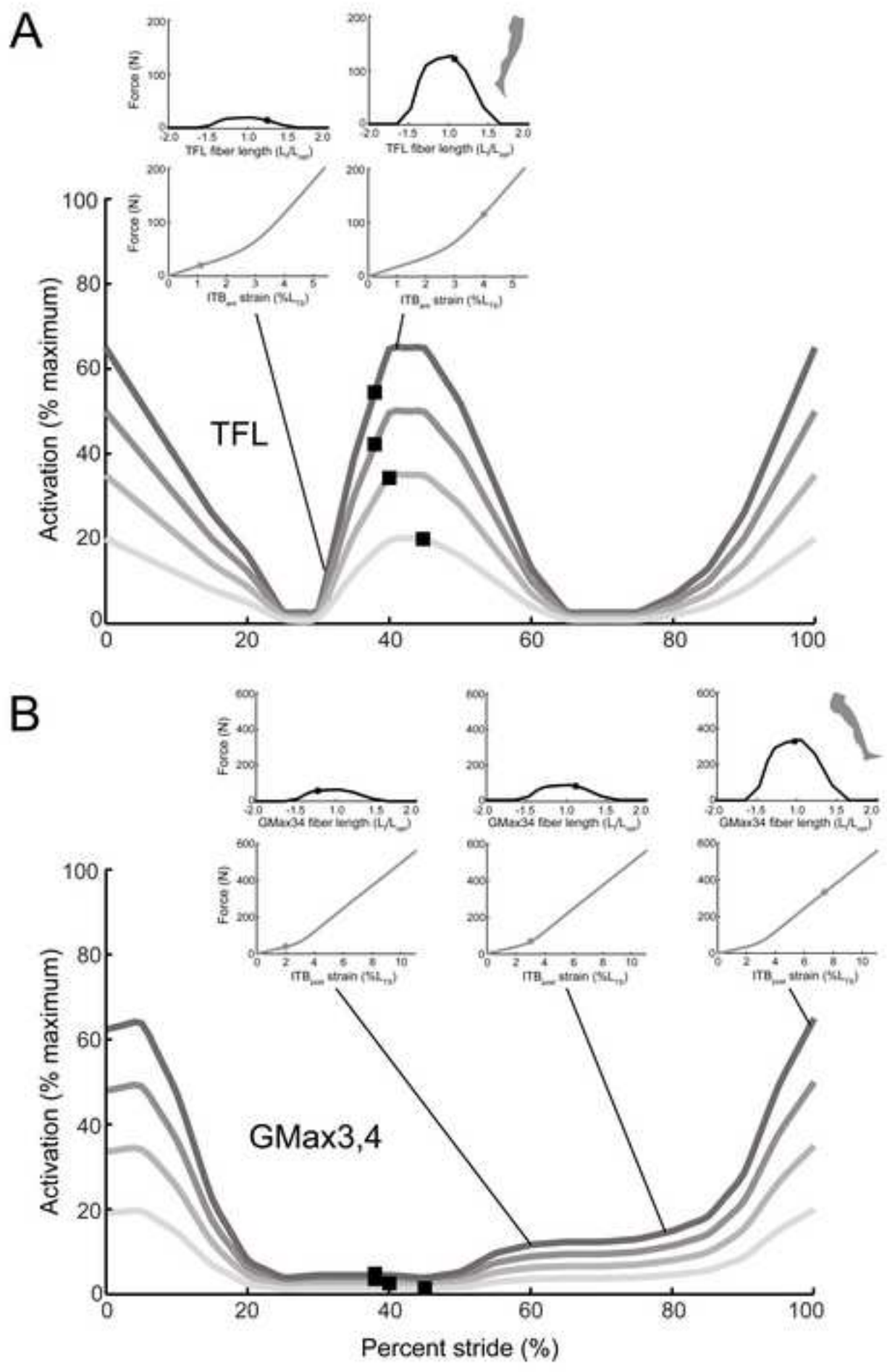

Figure 8

Click here to download high resolution image

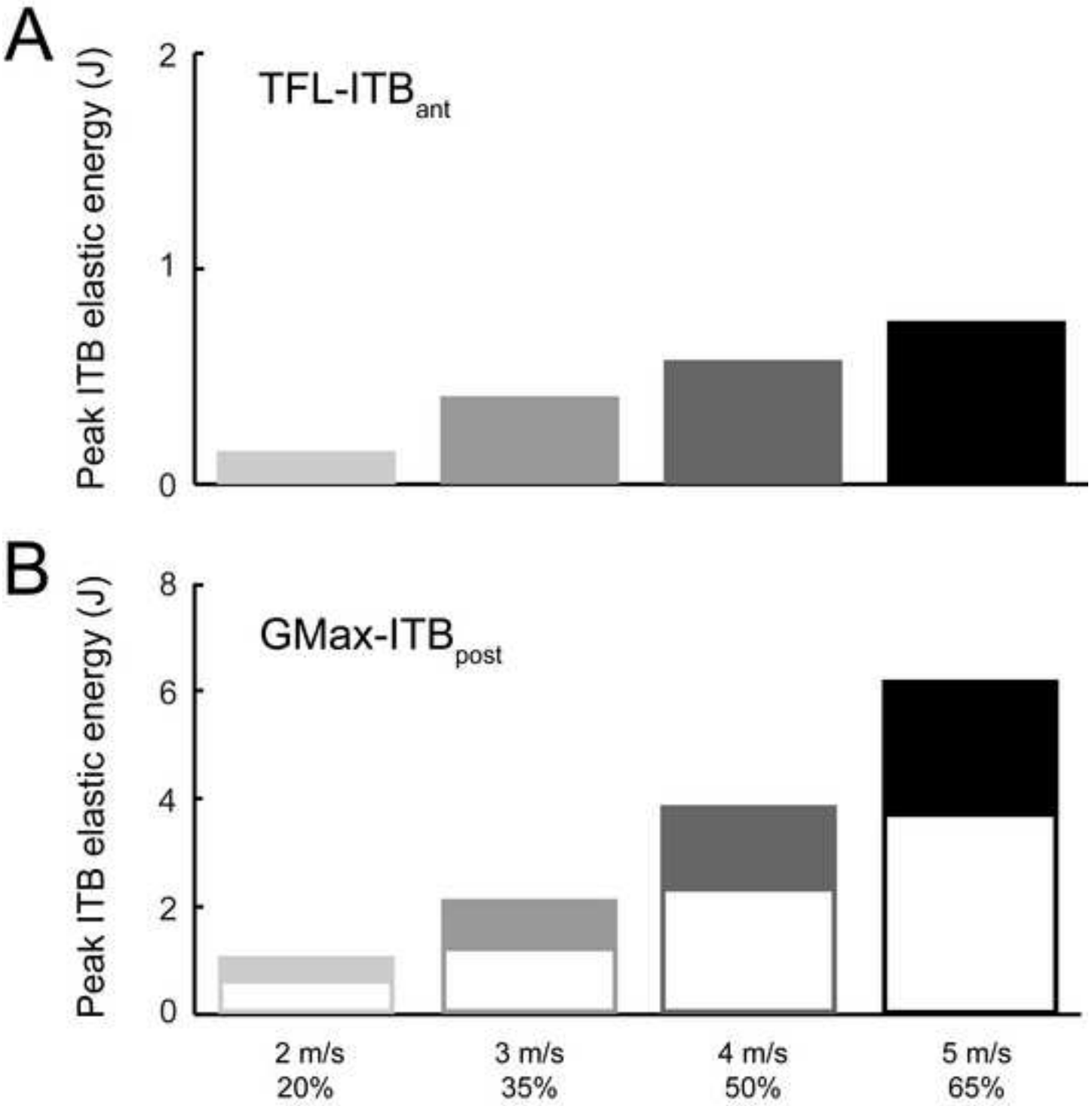

Figure S1

Click here to download high resolution image

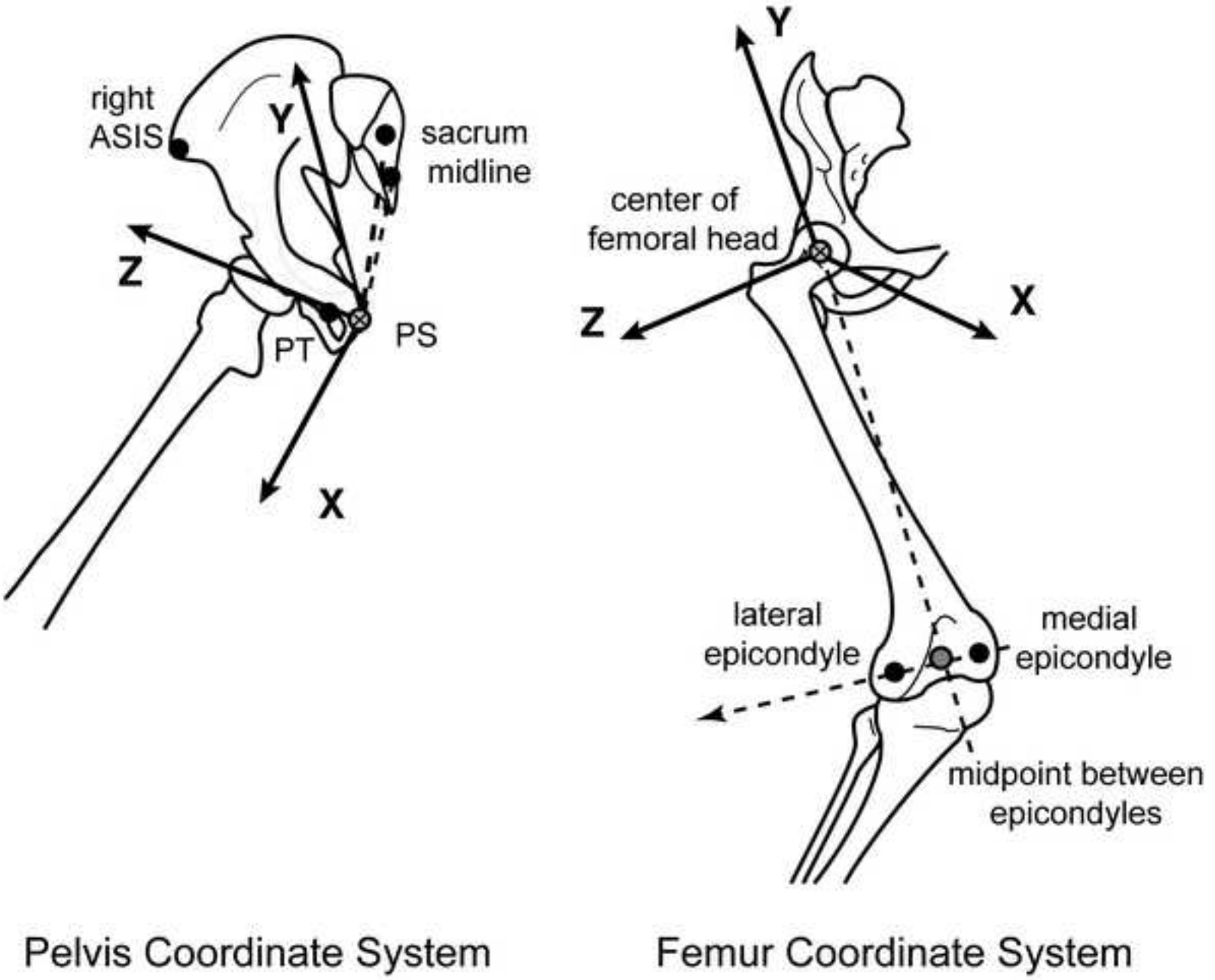

Figure S2

Click here to download high resolution image

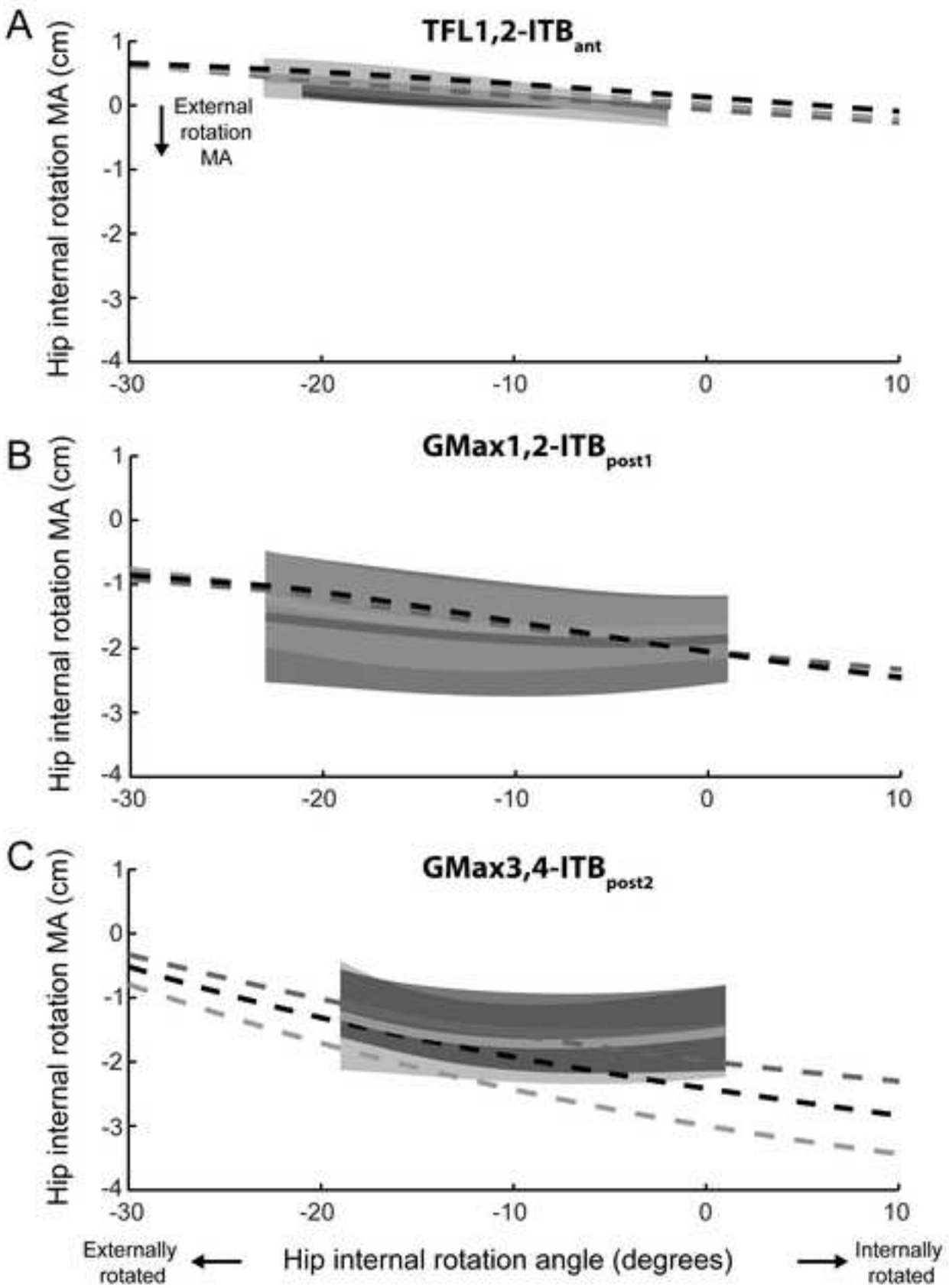

Table 1

Table 1. Muscle architecture of tensor fascia lata (TFL) and gluteus maximus (GMax*)

Muscle	Mass (g)	Optimal fascicle length (cm)	Pennation angle (deg.)	PCSA¥ (cm^2)
TFL	35.5 ± 9.6	9.8 ± 0.7	1.1 ± 1.1	3.2 ± 1.0
GMax	412.1 ± 69.7	14.4 ± 0.7	26.3 ± 5.0	30.6 ± 5.1

Data from 3 elderly cadaveric specimens (2 male, 1 female; mean age: 78 ± 6 years) are expressed as mean ± s.e.m.
¥Pennation angle is not included in the PCSA calculation since our SIMM model multiplies PCSA, specific tension, and pennation angle to determine a muscle's maximum isometric force.

Table 2

Table 2. Muscle regional masses of tensor fascia lata (TFL) and gluteus maximus (GMax)

Muscle	**Total mass of region (g)** (n=5)	**Percentage of mass inserting on ITB (%)** (n=2)
TFL1[∞]	26.4 ± 7.2	100%
TFL2	21.4 ± 5.5	100%
GMax1[¥]	110.6 ± 26.2	44.6 ± 4.9%
GMax2	109.4 ± 24.8	52.7 ± 7.8%
GMax3	121.9 ± 19.8	47.7 ± 11.3%
GMax4	104.7 ± 29.7	71.7 ± 28.3%

Data from 5 adult males (mean age: 62 ± 10 years) are expressed as mean ± s.e.m.
[∞]TFL was divided into two anterior-posterior regions based on origin and fascicle orientation.
[¥]GMax was separated into four superior-inferior regions.

Table S1

Table S1. Parameters used to scale a generic Hill-type muscle model to TFL- and GMax-ITB muscle-tendon units

Muscle-tendon unit	Maximum isometric force (N; F_{max})[¥]	Optimal fiber length (cm; L_{opt})	Pennation angle (deg; θ)	Tendon slack length (cm; L_{TS})
TFL1,2-ITB$_{ant}$[$]	195.2	9.8	2.5	42.6
GMax1,2-ITB$_{post1}$[*]	455.9	15.2	26.3	42.3
GMax3,4-ITB$_{post2}$[*]	558.6	16.7	26.3	41.0

[$] TFL *PCSA*, L_{opt}, and θ and GMax PCSA and θ from our measurements.
[*] GMax L_{opt} from Ward et al. (2009).
[¥] Fmax calculated as the product of *PCSA* and muscle specific tension of 61 N/cm^2 used by Arnold et al. (2010).

Table S2

Table S2. ITB thickness and width measurements used to calculate effective cross-sectional area and stiffness of each region

ITB Region	Thickness (mm)*	Width (mm)
ITB_{ant}	0.87 ± 0.34	16.35 ± 2.03
ITB_{post1}	0.97 ± 0.12	16.85 ± 1.85
ITB_{post2}		15.33 ± 1.86

Data from 3 elderly cadaveric specimens (2 male, 1 female; mean age: 78 ± 6 years) are expressed as mean ± s.e.m.
*Thicknesses of anterior and posterior regions were measured at proximal, middle, and distal sites and averaged across sites.